

MIT Open Access Articles

The Stable 3D Zn Electrode for High-Power Density Zn Metal Batteries

The MIT Faculty has made this article openly available. **Please share** how this access benefits you. Your story matters.

Citation: Zhu, Yun Guang, Narayanan, Thaneer Malai, Katayama, Yukihsa and Shao-Horn, Yang. 2021. "The Stable 3D Zn Electrode for High-Power Density Zn Metal Batteries." Journal of the Electrochemical Society, 168 (12).

As Published: 10.1149/1945-7111/ac4189

Publisher: The Electrochemical Society

Persistent URL: <https://hdl.handle.net/1721.1/141376>

Version: Final published version: final published article, as it appeared in a journal, conference proceedings, or other formally published context

Terms of Use: Article is made available in accordance with the publisher's policy and may be subject to US copyright law. Please refer to the publisher's site for terms of use.



The Stable 3D Zn Electrode for High-Power Density Zn Metal Batteries

To cite this article: Yun Guang Zhu *et al* 2021 *J. Electrochem. Soc.* **168** 120529

View the [article online](#) for updates and enhancements.



The Electrochemical Society
Advancing solid state & electrochemical science & technology

242nd ECS Meeting

Oct 9 – 13, 2022 • Atlanta, GA, US

Abstract submission deadline: **April 8, 2022**

Connect. Engage. Champion. Empower. Accelerate.

MOVE SCIENCE FORWARD




Submit your abstract





The Stable 3D Zn Electrode for High-Power Density Zn Metal Batteries

Yun Guang Zhu,¹ Thaneer Malai Narayanan,² Yukihiisa Katayama,³ and Yang Shao-Horn^{1,2,4,*} 

¹Research Laboratory of Electronics, Massachusetts Institute of Technology, Cambridge, Massachusetts 02139, United States of America

²Department of Mechanical Engineering, Massachusetts Institute of Technology, 77 Massachusetts Avenue, Cambridge, Massachusetts 02139, United States of America

³Production Engineering Development & Project Management Div. Powertrain Company, 471-8571, Japan

⁴Department of Material Science and Engineering, Massachusetts Institute of Technology, 77 Massachusetts Avenue, Cambridge, Massachusetts 02139, United States of America

A stable Zn metal electrode can develop rechargeable zinc metal batteries (RZMBs) which have the high theoretical capacity (820 mAh g⁻¹), low redox potential, and intrinsic safety. However, the corrosion of Zn metal in aqueous electrolytes and Zn dendrite formation during the plating process lead to poor cycling and thus hinder the development of RZMBs. Here, we employed ionic liquid-based gel polymer (poly(vinylidene fluoride)-co-hexafluoropropylene, PVDF-HFP) and acetylene black (AB) to achieve a stable and flexible three-dimensional (3D) Zn/AB/PVDF-HFP film electrode with ionic and electronic conductive networks and high surface area, showing 26 times higher plating/stripping current than planar Zn plate. By developing a continuous structure between the ionic liquid-based gel polymer membrane and the flexible 3D Zn/AB/PVDF-HFP electrode, the low resistance, high rate capability and long cycle life (> 800 h) was obtained. Our work shows a flexible Zn film electrode and ionic liquid-based gel polymer electrolyte, could pave the path for rechargeable and high-cycle life thin-film RZMBs.
© 2021 The Electrochemical Society ("ECS"). Published on behalf of ECS by IOP Publishing Limited. [DOI: 10.1149/1945-7111/ac4189]

Manuscript submitted October 19, 2021; revised manuscript received November 28, 2021. Published December 20, 2021. *This paper is part of the JES Focus Issue on Focus Issue In Honor of John Goodenough: A Centenarian Milestone.*

Supplementary material for this article is available [online](#)

To meet the requirements of electric vehicles (EVs), research institutes and industries focus on developing high-energy density Li-ion batteries.¹ Compared to lithium-ion batteries, a rechargeable zinc metal batteries (RZMBs) which uses Zn as an anode in non-flammable electrolytes are a promising candidate given its advantages such as cost-effectiveness, good safety, and high energy density.² However, the Zn anode shows poor cycle life in aqueous electrolytes due to the corrosion and the dendrite formation.² Several methods have been reported to prevent the Zn dendrite formation, such as electrolyte modification,³⁻⁵ Zn metal modification,⁶⁻⁹ a novel charge-discharge scenario for Zn plating/stripping¹⁰. For example, concentrated aqueous electrolytes (e.g., 1 m Zn(TFSI)₂ + 20 m LiTFSI) are shown to increase the cycling stability of Zn metal because no water is present in the Zn²⁺-solvation sheath for H₂ evolution.⁵ However, the high cost of concentrated electrolytes may hinder their practical application. Some types of local-concentrated electrolytes have been designed for Li-ion batteries to lower the cost.^{11,12} However, the narrow electrochemical window of aqueous electrolytes not only leads to poor cycling stability of the Zn anode but also hinders the exploration of high voltage cathodes for RZMBs. Therefore, it is critical to explore alternative non-aqueous electrolytes for RZMBs. Gel-polymer electrolytes containing both liquids and solid polymers with high conductivity have been widely studied for Li-ion batteries,^{13,14} Na-ion batteries,^{15,16} and Zn-ion batteries.¹⁷⁻¹⁹ Among these non-aqueous electrolytes, ionic liquids have attracted lots of attention due to their high thermal stability, high conductivity, wide stable window, etc, which can extend the application of RZMBs in harsh environments, such as aerospace, airplanes, or submarines.^{2,20}

The structure of the Zn metal anode is also critical for the development of RZMBs. Zn planar metal is the most common Zn anode in RZMBs, but it limits the surface area available for plating and the battery's structural flexibility.²¹ By overcoming these disadvantages, one could envision Zn electrode to have a high cycle life, and being a flexible electrode to be used as the structural battery

in EVs. Some groups have developed flexible, high surface-area and free-standing Zn anode in Zn-air batteries using Zn particles and polymer binders.^{22,23} However, these flexible Zn anodes are applied in alkaline aqueous electrolytes, which may cause corrosion due to the high surface area of Zn particles and usage of carbon conductive additives.²⁴ Ionic liquid electrolytes can be a good candidate for high surface area Zn anode due to their high electro(chemical) stability.²⁰ Therefore, we design a flexible Zn film electrode with ionic (ionic liquid-based gel polymer) and electronic networks (carbon/Zn particles).

Here, we employed the ionic liquid (1-Ethyl-3-methylimidazolium bis(trifluoromethylsulfonyl)imide, EMIMTFSI)-based gel polymer (poly(vinylidene fluoride)-co-hexafluoropropylene, PVDF-HFP) electrolyte as both the Zn-ion conducting membrane and binder in the Zn film electrode. Although the low-cost 1-Ethyl-3-methylimidazolium chloride (EMICl) should be another potential ionic liquid for the gel polymer electrolyte the higher operation temperature (>100 °C) may limit its application.²⁵ In the flexible three-dimensional (3D) Zn film electrode (Zn/AB/PVDF-HFP), the acetylene black (AB) and the ionic liquid (EMIMTFSI)-based gel polymer (PVDF-HFP) were used to enable the electronically conductive network, and the ionically conductive binder, respectively. Due to the good stability of Zn particles in the ionic liquid (EMIMTFSI)-based gel polymer (PVDF-HFP) electrolyte (GPE), the Zn/AB/PVDF-HFP symmetric cell showed long cycle life (> 800 h). The high specific surface area of effective Zn particles in the Zn/AB/PVDF-HFP electrode provides ~26 times higher reactivity than the planar Zn metal electrode and high rate capability (up to 10 mA cm⁻²_{geo.}). The excellent electrochemical performance of Zn/AB/PVDF-HFP symmetric cells provides new opportunities to enable the development of thin-film RZMBs, which could be used as structural batteries for buildings and EVs.

Experimental

Materials.—Poly(vinylidene fluoride-co-hexafluoropropylene) (PVDF-HFP, MW ~455000, Sigma Aldrich) is used as the raw materials to prepare PVDF-HFP membranes. Acetone (99.9%, Sigma Aldrich) is used as the solvent to dissolve PVDF-HFP for

*E-mail: shaohorn@mit.edu

membrane casting. Acetylene black (100% compressed, Strem Chemical Inc.) and zinc powder (6–9 μm , 97.5%, Alfa Aesar) are used to prepare Zn electrodes. Zinc(II) Bis(trifluoromethanesulfonyl) imide (Zn(TFSI)_2 , $\geq 98\%$, TCI America) and 1-Ethyl-3-methylimidazolium bis(trifluoromethylsulfonyl)imide (EMIMTFSI, $\geq 99\%$, Sigma Aldrich) are used as ionic liquid electrolyte for PVDF-HFP swelling.

Preparation of PVDF-HFP membrane.—0.5 g of PVDF-HFP pellets were stirred and dissolved in 4.5 ml acetone at 50 $^\circ\text{C}$ for 2 h. 2 ml of the above solution was transferred into a glass module ($2.54 \times 2.54 \text{ cm}^2$). The PVDF-HFP membrane formed after 1 h at room temperature. Then the casted membrane was dried in a Büchi vacuum glass oven at 100 $^\circ\text{C}$ for 12 h. After drying, the membrane was transferred into the Ar-filled glove box for use. For the gelation, the dry PVDF-HFP membrane was immersed into 0.1 M $\text{Zn(TFSI)}_2/\text{EMIMTFSI}$ electrolyte at 60 $^\circ\text{C}$ for 12 h. The PVDF-HFP gel membranes were wiped using Kimtech papers to remove the residual electrolyte from the surface for battery assembling.

Preparation of Zn/AB/PVDF-HFP electrode.—0.2–0.5 g of PVDF-HFP pellets were stirred and dissolved in 4.5 g Acetone at 50 $^\circ\text{C}$ for 2 h. 0.2 g of Acetylene black (AB) and 1.8 g of Zn particles with a specific surface area of $0.43 \text{ m}^2 \text{ g}^{-1}$ were grounded for 20 min. Then, the above grounded powder was transferred into the PVDF-HFP solution and stirred for overnight at 50 $^\circ\text{C}$. The uniform suspension was doctor blended as the Zn/AB/PVDF-HFP film electrode with the gap of 100 μm . Then, the electrode was dried in a Büchi vacuum glass oven at 100 $^\circ\text{C}$ for 12 h. After drying, the membrane was transferred into the Ar-filled glove box for use. For the gelation, the dry Zn/AB/PVDF-HFP film electrode was immersed into 0.1 M $\text{Zn(TFSI)}_2/\text{EMIMTFSI}$ electrolyte at 60 $^\circ\text{C}$ for 12 h. The gelled Zn/AB/PVDF-HFP film electrode was wiped using Kimtech papers to remove the residual electrolyte from the surface for battery assembling.

Zn symmetric battery assembling and testing.—Two pieces of Zn/AB/PVDF-HFP film electrodes with a diameter of 1.27 cm were separated by a piece of PVDF-HFP gel membrane. The above sandwich symmetric components were put into a Tome-type cell with stainless steel plates as the current collectors. Electrochemical impedance spectroscopy (EIS) measurements were performed with a frequency range from 10 Hz to 1 MHz and voltage amplitude of 10 mV in an environment chamber at different temperatures (–20 to 70 $^\circ\text{C}$). The galvanostatic charge/discharge measurements were conducted at room temperature at current densities from 1 to 2 mA cm^{-2} . The cyclic voltammetry measurements were performed at room temperature at the scanning rate of 10 mV s^{-1} in the potential range from –0.5 to 0.5 V. The control cells were assembled and tested with Zn plates as the active electrodes. All the above electrochemical measurements were conducted after 12 h of rest for cell stabilization.

Characterizations of materials.—The PVDF-HFP membrane and Zn/AB/PVDF-HFP film electrode were characterized using X-ray diffraction (XRD, Bruker D2 Phaser), Raman spectroscopy (HORIBA Scientific LabRAM HR800), and scanning electron microscope (SEM, Zeiss Merlin). The cross-section film samples were broken after quenching in the liquid nitrogen. In XRD measurements, the applied voltage and current are 30 kV and 10 mA, respectively, using $\text{Cu-K}\alpha$ radiation ($\lambda = 1.54178 \text{ \AA}$). In the Raman spectra measurements, a red laser ($\lambda = 632.8 \text{ nm}$) was used with 50-fold magnification. An exposure time of 15 s with 600 grating was used, and each spectrum was accumulated 5 times. The cycled Zn/AB/PVDF-HFP and planar Zn electrodes were washed using anhydrous acetonitrile (ACN) three times and then dried in a vacuum oven at room temperature.

Results and Discussion

To make a 3D Zn electrode, we used PVDF-HFP polymer as the binder and acetylene black (AB) as the electronically conductive additive to make the well-connected network (Fig. S1 (available online at stacks.iop.org/JES/168/120529/mmedia)), which could provide good electronic conductivity ($\sim 1 \text{ mS cm}^{-1}$, Fig. S2), as shown in schematic structure (Fig. 1). In the casted Zn/AB/PVDF-HFP film electrode, Zn particles were well dispersed in the AB/PVDF-HFP network (Fig. S1). After gelation in 0.1 M $\text{Zn(TFSI)}_2/\text{EMIMTFSI}$ ionic liquid electrolyte, the Zn^{2+} , EMIM⁺, and TFSI[–] were absorbed in the PVDF-HFP 3D network, resulting in 3D ionic conductive channels in the Zn/AB/PVDF-HFP electrode. The PVDF-HFP network can also provide a compatible interface between the Zn/AB/PVDF-HFP electrode and PVDF-HFP membrane, resulting in a long cycling life (> 800 h) with high geometric current densities (1–10 mA $\text{cm}^{-2}_{\text{geo}}$) without performance decay, which will be discussed in the following sections. To integrate our designed 3D Zn electrode and gel-polymer electrolyte, the ideal cathode should be a Zn-ion intercalation material, which could ideally realize a rocking-chair battery like conventional Li-ion batteries. Unfortunately, there is still no ideal Zn cathode materials reported based on our best knowledge. Except for the Zn-ion intercalation cathodes, the other options are these active materials with conversion reactions, like oxygen²⁶ and sulfur electrode²⁷.

The PVDF-HFP membrane was cast on the glass module with a thickness of $30 \pm 10 \mu\text{m}$, as shown in the cross-section SEM image (Fig. 2a). Although a few small pores (<100 nm) were found on the PVDF-HFP membrane in Fig. 2b, they are not through-holes as indicated in the cross-section image (Fig. 2a). Therefore, the dense membrane could absorb electrolytes to form a gel polymer network but not store electrolytes in pores. After gelation, the white dry PVDF-HFP membrane (Fig. 2c) becomes slightly transparent (Fig. 2d). Through Raman spectra shown in Fig. 2e, there are the peaks from both EMITFSI and Zn(TFSI)_2 , indicating the absorption of electrolytes (0.1 M Zn(TFSI)_2 in EMITFSI) in the PVDF-HFP membrane after gelation. The swelling ratio (SR) of the GPE was

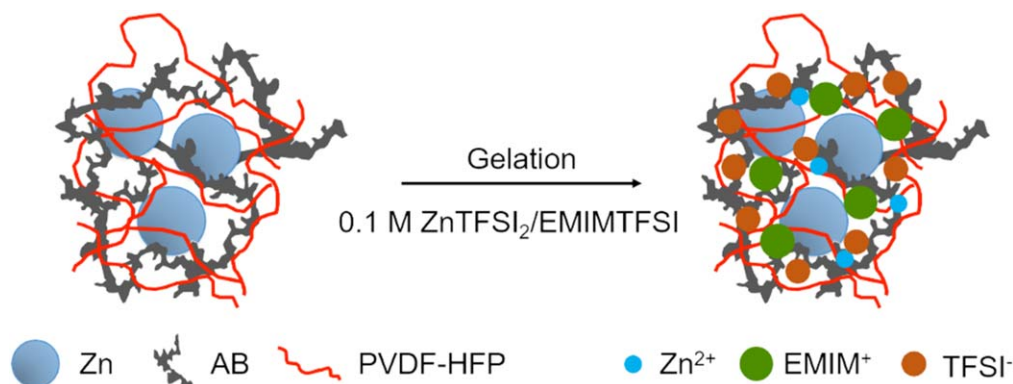


Figure 1. The schematic structure of Zn/AB/PVDF-HFP electrode and the gelation process in 0.1 M $\text{Zn(TFSI)}_2/\text{EMIMTFSI}$ ionic liquid electrolyte.

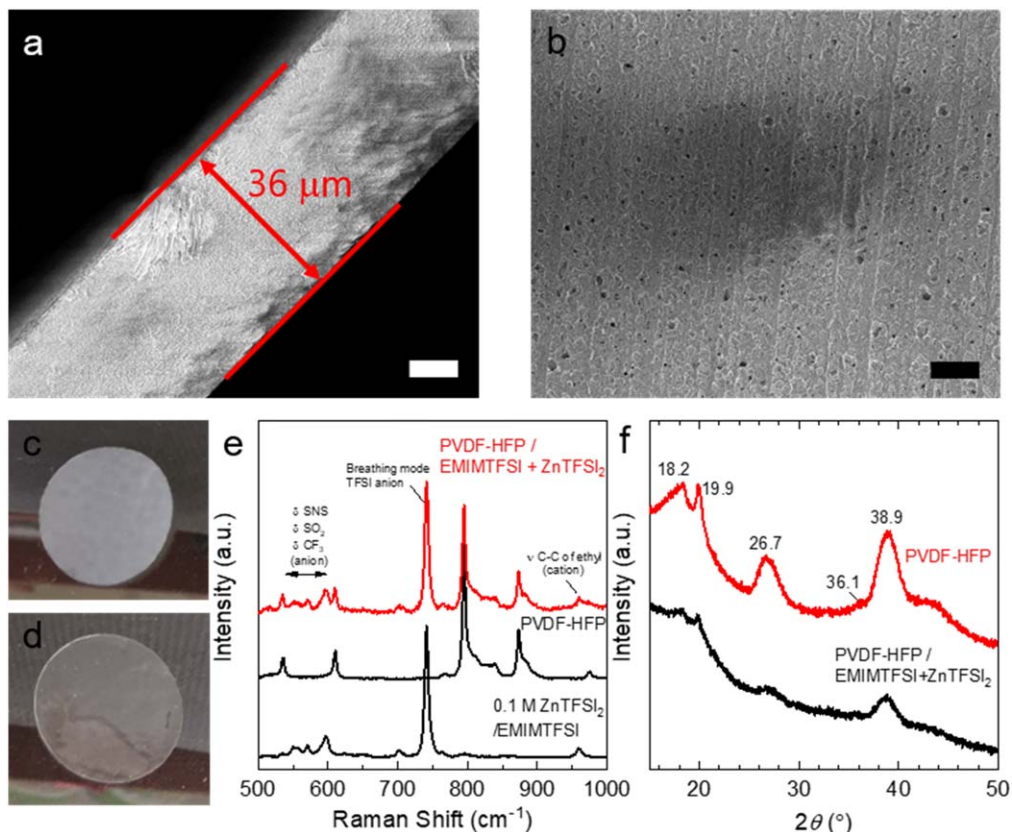


Figure 2. (a)–(b) The SEM images of cross-section (a) and the surface morphology (b) of a dry PVDF-HFP membrane. The scale bar is 10 μm . (c)–(d) The photos of a dry PVDF-HFP membrane (1.27 cm^2 of diameter) (c) and a swelled one (d). (e) The Raman spectra of 0.1 M ZnTFSI₂/EMIMTFSI, the PVDF-HFP membrane, and the membrane after swelling (PVDF-HFP/EMIMTFSI + ZnTFSI₂). (f) The XRD patterns of the PVDF-HFP membrane and the membrane after swelling (PVDF-HFP/EMIMTFSI + ZnTFSI₂). In the gelation process, the PVDF-HFP membrane was immersed in 0.1 M ZnTFSI/EMIMTFSI ionic liquid at 50 $^{\circ}\text{C}$ for 12 h in the Ar-filled glove box.

obtained according to Eq. 1, which is $61 \pm 3\%$. Through XRD measurements in Fig. 2f, the main phase structure of casted PVDF-HFP film is α -phase due to the two clear peaks at 18.2 $^{\circ}$ and 19.9 $^{\circ}$.²⁸ After gelation in 0.1 M ZnTFSI/EMIMTFSI at 50 $^{\circ}\text{C}$ for 12 h, all these feature peaks are decreased, indicating the decrease of crystallinity.

$$\text{SR} = (m_g - m_d)/m_d \quad [1]$$

Where m_g and m_d are weights of the dry PVDF-HFP films and after swelling, respectively. The samples were immersed in 0.1 M ZnTFSI/EMIMTFSI ionic liquid at 50 $^{\circ}\text{C}$ for 12 h in the Ar-filled glove box.

In order to increase the active surface area and the flexibility of a Zn electrode, we made a flexible 3D Zn electrode using AB as the electronic conductive network and PVDF-HFP as both the binder and ionic conductive network. As shown in Figs. 3a and 3b, Zn particles are uniformly anchored in the AB and PVDF-HFP (20 w%) networks. In addition, as we change the amount of PVDF-HFP from 9.1 w% to 20 w%, the electronic conductivities of these electrodes (Fig. S2) do not change much. However, with increasing the PVDF-HFP, more Zn particles appear on the surface of the Zn/AB/PVDF-HFP electrode, as shown in Fig. S1. To make sure that Zn particles are stably anchored in the PVDF-HFP network, we chose the electrode with 20 w% of PVDF-HFP for the electrochemical measurements (Fig. S1). The thickness of the Zn/AB/PVDF-HFP electrode is 22 μm based on the SEM image of the cross-section (Fig. 3c). The electrode also shows a homogeneous distribution of Zn particles vertically, indicating the Zn/AB/PVDF-HFP suspension's high mechanical stability (i.e. no disintegration or sedimentation due to gravity) during the casting process. There are several peaks from Zn and PVDF-HFP through XRD measurements in

Fig. 3d. There is a small amount of ZnO in the Zn/AB/PVDF-HFP electrode but not in the pristine Zn powder, which may be from the corrosion of the Zn particles during the suspension preparation.

The symmetric Zn/AB/PVDF-HFP cell was assembled which schematic structure is shown in Fig. 4a. From the Nyquist plot at 25 $^{\circ}\text{C}$ in Fig. 4b, the clear semi-circle (~ 13.4 ohm) is assigned to the impedance from PVDF-HFP gel polymer electrolyte, showing the ionic conductivity is $1.1 \times 10^{-4} \text{ S cm}^{-1}$. Liu et al. demonstrated Zinc trifluoromethanesulfonate (Zn(Tf)₂)/PVDF-HFP polymer electrolyte without ionic liquid, showing around a lower ionic conductivity ($\sim 2.4 \times 10^{-5} \text{ S cm}^{-1}$).²⁹ Adding EMITF can enhance the conductivity of the Zn(Tf)₂/PVDF-HFP polymer electrolyte up to $1.4 \times 10^{-4} \text{ S cm}^{-1}$.³⁰ Adding organic solvents (e.g., propylene carbonate (PC), ethylene carbonate (EC))³¹ or porous inorganic particles (e.g. SiO₂)³² can realize the conductivity of the order of $10^{-3} \text{ S cm}^{-1}$. The first intersection point shows the low contact resistance (~ 1.7 ohm), indicating the good electronic conductivity ($8.5 \times 10^{-4} \text{ S cm}^{-1}$) of the Zn/AB/PVDF-HFP electrode. However, the Zn plate symmetric cell with the PVDF-HFP gel polymer shows a much higher interface resistance ($> 5 \times 10^4$ ohm, Fig. S3), which resulted in the poor electrochemical performance as shown in the later section. As shown in Fig. 4c, the ionic conductivity of the PVDF-HFP gel polymer electrolyte with the temperature obeys the Vogel-Tammann-Fulcher (VTF) behavior throughout the temperature range from -20 to 70 $^{\circ}\text{C}$, and they are fitted to the equation:

$$\sigma = AT^{-1/2} \exp\left(-\frac{E_a}{K_B(T - T_0)}\right) \quad [2]$$

Where A is the pre-exponential factor, E_a is the activation energy, K_B is the Boltzmann constant, T is the testing temperature, and T_0 is

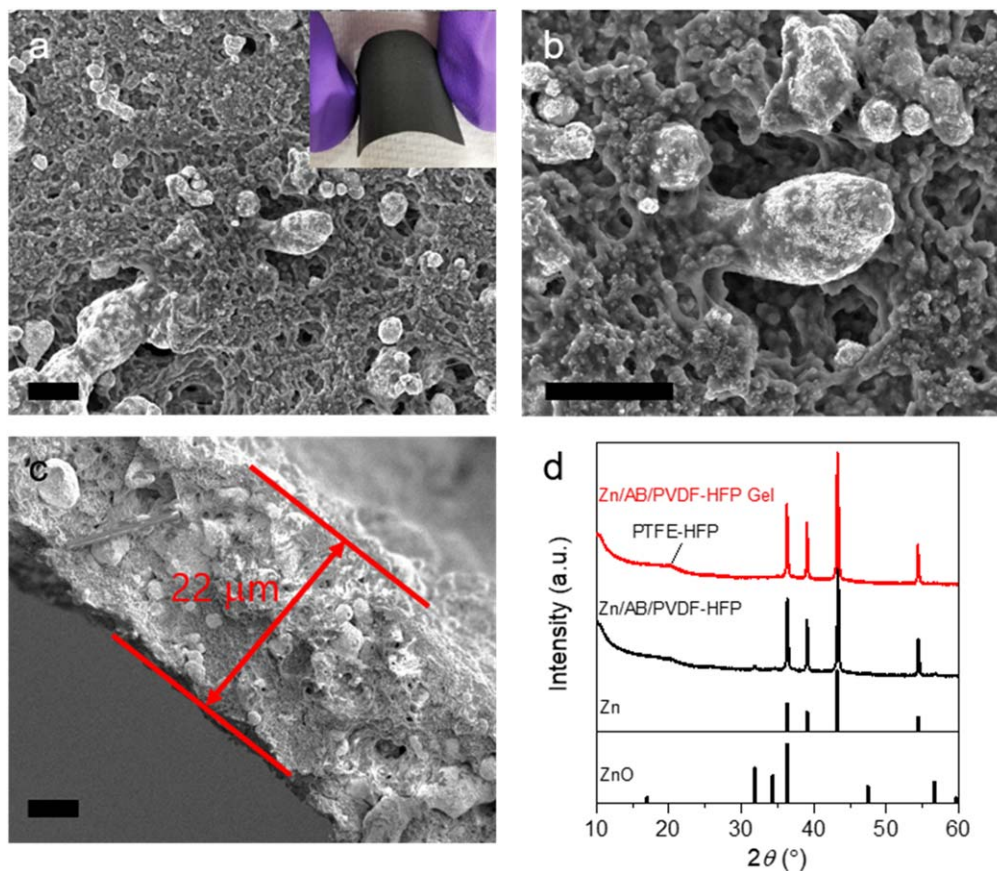


Figure 3. The SEM images of the Zn/AB/PVDF-HFP electrode (a) and (b). The inset of (a) shows the photo of the flexible Zn/AB/PVDF-HFP electrode. (c) The SEM image of the cross-section of the Zn/AB/PVDF-HFP electrode. The scale bar is 5 μm . (d) The XRD patterns of the flexible Zn/AB/PVDF-HFP electrode (in black) and the one after gelation (in red). The standard XRD references are Zn (ICDD# 04-003-7274) and ZnO (ICDD# 04-023-7335).

the equilibrium glass transition temperature, which is deduced from the Eq. 3³³.

$$T_0 = T_g - 50 \text{ K} \quad [3]$$

Where the glass transition point T_g of EMIMTFSI is 175 K³⁴.

The VFT behavior has been largely reported for ionic liquid electrolytes.³⁵⁻³⁷ The activation energy (E_a) is 0.03 eV from the fitting results, which is comparable to the previously reported value (0.03 eV) for PVDF-HFP + EMIMTFSI gel electrolyte.³⁸

The cyclic voltammetry (CV) curves in Fig. 4d shows the good reversibility of Zn plating/stripping in ionic liquid (0.1 M ZnTFSI₂/EMIMTFSI) based GPE for both the Zn/AB/PVDF-HFP electrode and the planar Zn metal electrode, indicating that the high stability of Zn against the GPE. The oxidation/reduction current density of the Zn/AB/PVDF-HFP electrode is $\sim 0.17 \text{ mA cm}^{-2}_{\text{geo}}$, which is ~ 26 times higher than that of a planar Zn metal electrode. The high kinetics of the Zn/AB/PVDF-HFP electrode is attributed to the high surface area of Zn particles. The reversibility and stability of the Zn/AB/PVDF-HFP electrode were investigated using symmetric cell at constant currents, as shown in Fig. 4e. After cycling over 840 h (100 cycles at $1 \text{ mA cm}^{-2}_{\text{geo}}$, 400 cycles at $2 \text{ mA cm}^{-2}_{\text{geo}}$, 200 cycles at $4 \text{ mA cm}^{-2}_{\text{geo}}$, and 1000 cycles at $10 \text{ mA cm}^{-2}_{\text{geo}}$), the Zn/AB/PVDF-HFP symmetric cell still showed stable charge-discharge profiles. No obvious voltage plateau change in Zn stripping and plating process (Fig. S4), indicating that the conductivity of the cell doesn't change much in the Zn plating/stripping process. As a comparison, the Zn plate symmetric cell cannot be cycled at high currents (e.g., $1 \text{ mA cm}^{-2}_{\text{geo}}$) due to its low surface area and poor interface contact with GPE (Fig. 4f). At low currents of 0.01 and $0.02 \text{ mA cm}^{-2}_{\text{geo}}$, the Zn plate symmetric cell still showed high overpotentials. The utilization of Zn in the Zn/AB/PVDF-

HFP (Fig. 4e) and Zn planar electrodes (Fig. 4f) in the charge/discharge process are $\sim 51\%$ and $3 \times 10^{-3}\%$, respectively. In the recent studies, the Zn foil electrodes in aqueous (e.g. $1 \text{ M Zn}(\text{CF}_3\text{SO}_2)_2 + 25 \text{ mM Zn}(\text{H}_2\text{PO}_4)_2$, $\text{ZnCl}_2-2.33\text{H}_2\text{O}$), non-aqueous ($1.0 \text{ M Zn}(\text{TFSI})_2$ in AN⁴¹), and polymer-based electrolytes (Zincic perfluorinated sulfonic acid membrane⁴², $\text{Zn}(\text{ClO}_4)_2$ /polyacrylamide⁴³) can achieved long cycling life ($>1000 \text{ h}$) at current density ranging from 0.1 to $5 \text{ mA cm}^{-2}_{\text{geo}}$. Compared with the reported work, our designed Zn/AB/PVDF-HFP electrode can achieve the highest current density ($10 \text{ mA cm}^{-2}_{\text{geo}}$), which could attribute to its higher effective surface area than planar Zn foil, as summarized in table S1. In short, the Zn/AB/PVDF-HFP symmetric cells, with high surface area, good contact with GPE, and good stability with ionic liquids, showed high reactivity, high-rate capability, and good cycling stability.

To further analyze Zn stripping and plating, we characterized the Zn/AB/PVDF-HFP electrode ($3.37 \text{ mg}_{\text{Zn}}/\text{cm}^2_{\text{geo}}$, $0.38 \text{ mg}_{\text{AB}}/\text{cm}^2_{\text{geo}}$, and $0.94 \text{ mg}_{\text{PVDF-HFP}}/\text{cm}^2_{\text{geo}}$) before and after cycling using SEM and EDS mapping. From the SEM images (Figs. S5b-S5d) of the pristine and cycled Zn/AB/PVDF-HFP electrode at current densities from $1-10 \text{ mA cm}^{-2}_{\text{geo}}$ (Fig. S5a), small Zn particles were plated on the electrode surface without Zn dendrites formation after cycling. The Zn/AB/PVDF-HFP electrode ($24 \mu\text{m}$, 4.28 mg of Zn) has an active surface area of 13 cm^2 , which is ~ 10 times higher than the geometric surface area of the planar Zn plate (1.27 cm^2 , 181 mg). The current density required for Zn dendrite formation within a given time can be estimated from Sand's relationship.⁴⁴ Hence, if dendrite forms at $0.5 \text{ mA cm}^{-2}_{\text{geo}}$, within 1 h for a planar electrode, it takes $5 \text{ mA cm}^{-2}_{\text{geo}}$ for dendrites to develop on Zn/AB/PVDF-HFP electrode surface within the same time. The required current density can be increased by increasing the volume fraction of Zn or by increasing the thickness of Zn/AB/

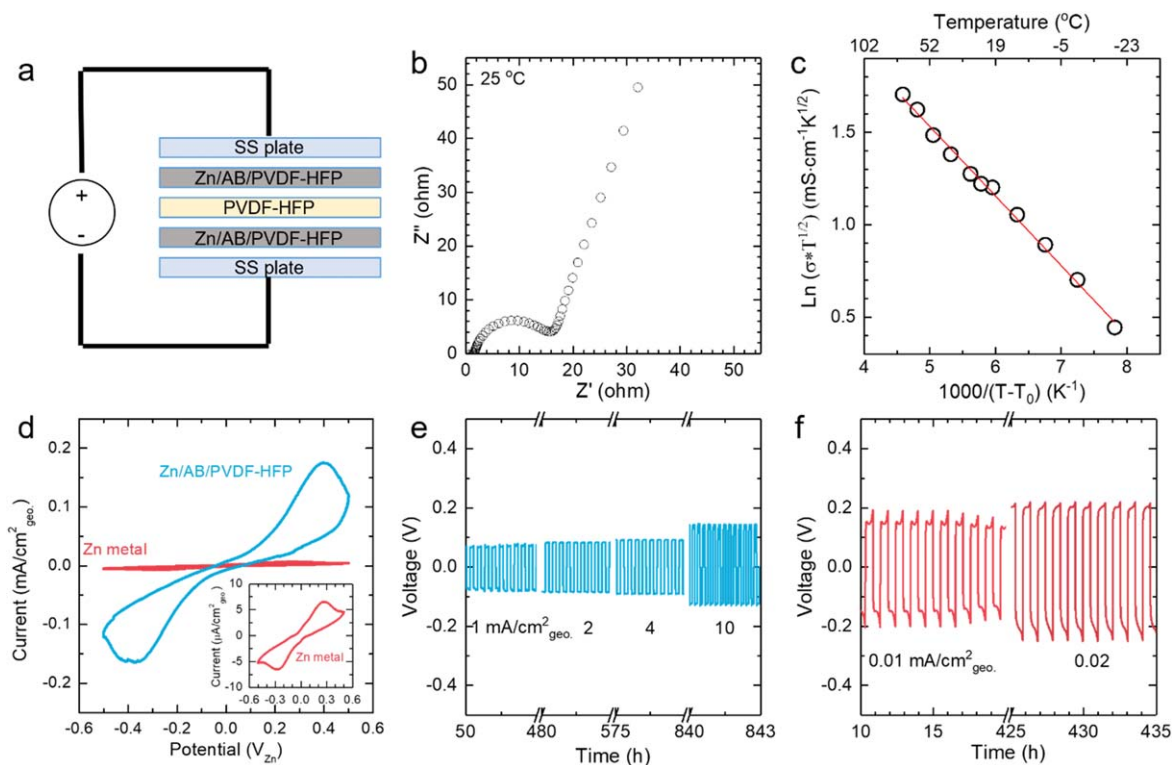


Figure 4. (a) The Zn/AB/PVDF-HFP symmetric cell's schematic structure for electrochemical performance testing. (b) The Nyquist plot is the Zn/AB/PVDF-HFP symmetric cell with a voltage bias of 10 mV with a frequency range from 1 MHz to 10 Hz. (c) Variation of ionic conductivity of the PVDF-HFP gel polymer electrolyte with temperature. (d) Cyclic voltammetry (CV) curves of Zn plating and stripping in Zn/AB/PVDF-HFP and planar Zn metal symmetric cells at a scan rate of 10 mV s^{-1} . The galvanostatic charge/discharge profiles of a Zn/AB/PVDF-HFP symmetric cell (e) at currents of 1, 2, 4, and $10 \text{ mA cm}^{-2}_{\text{geo}}$, and a planar Zn metal symmetric cell (f) at currents of 0.01 and $0.02 \text{ mA cm}^{-2}_{\text{geo}}$. The thickness of the Zn/AB/PVDF-HFP electrodes in the cell is $\sim 24 \mu\text{m}$. The thickness of Zn plate is $\sim 200 \mu\text{m}$.

PVDF-HFP electrode. Therefore, zinc dendrite formation can be prevented in the Zn/AB/PVDF-HFP electrode. The SEM images (Figs. S5f–S5h) of the pristine and cycled Zn metal electrode (Fig.

S5e) suggest that Zn stripping/plating happened along the Zn metal grain boundaries. Due to the low current densities (0.01 and $0.02 \text{ mA cm}^{-2}_{\text{geo}}$) and shallow cycling capacity (up to $0.01 \text{ mAh cm}^{-2}_{\text{geo}}$) in

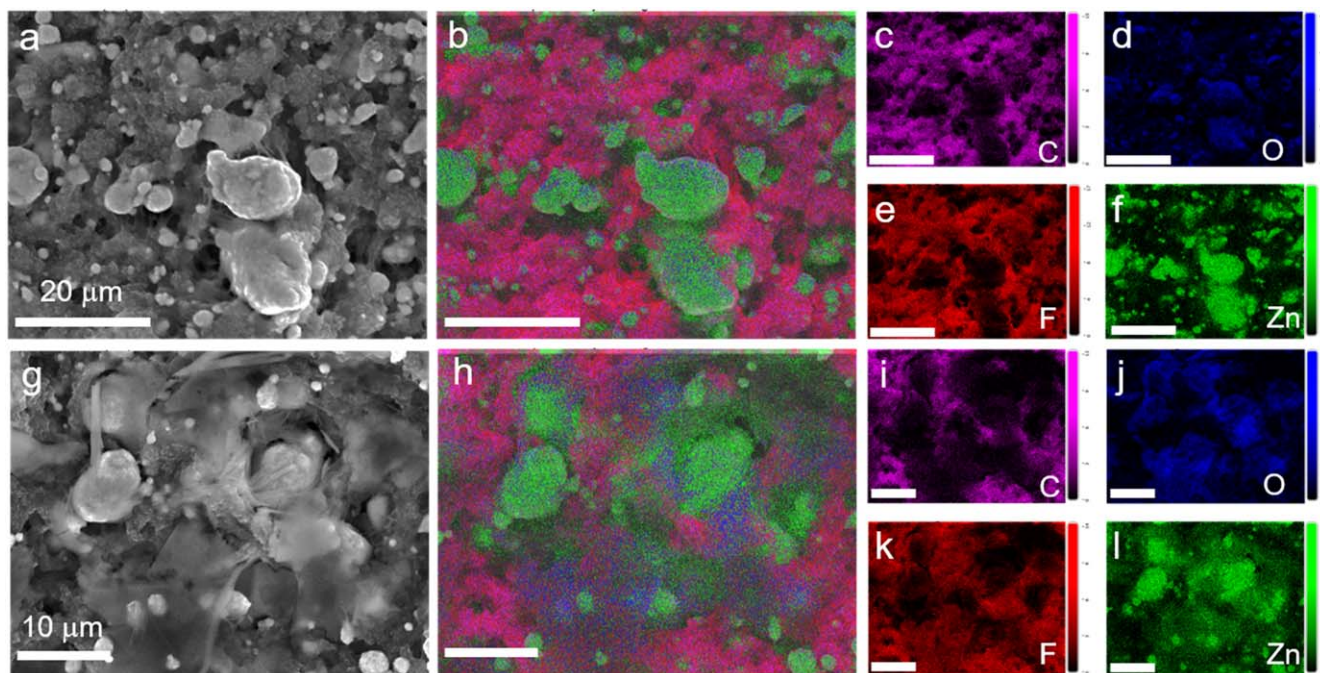


Figure 5. The SEM images and EDS mapping images of pristine (a)–(f) and cycled Zn/AB/PVDF-HFP electrodes (g)–(l). Layered images combining all four elements mapping (b), (h). EDS maps of C K (c), (i), O K (d), (j), F K (e), (k) and Zn K (f), (l). The cycled Zn/AB/PVDF-HFP electrode was collected from the one after cycling for more than 800 h (Fig. 4e).

Fig. 4f, there was no Zn dendrite formation on the Zn metal electrode after cycling. In Figs. 5a–5f, we could note that there are clear boundaries between Zn particles and AB or PVDF-HFP networks in the pristine electrode. With a homogeneous distribution of Zn particles in AB and PVDF-HFP networks, the Zn/AB/PVDF-HFP electrode showed high electronic ($\sim 1 \text{ mS cm}^{-1}$) and ionic conductivities ($\sim 0.1 \text{ mS cm}^{-1}$) at room temperature. After cycling in Figs. 5g–5l, the boundary of Zn particles in the electrode become blur and lots of small Zn particles appear on the electrode surface. The above results could support that the Zn plating not only happens on the Zn particles but also on the carbon particles. Therefore, the Zn/AB/PVDF-HFP electrode has an even more electrochemically active surface area with increasing cycling number because more and more AB surfaces will be utilized as the active sites for Zn plating and stripping. Although we didn't observe the obvious degradation of the 3D Zn electrode, it is worth discussing the potential degradation. Firstly, the potential degradation may be from the Zn corrosion if the battery is contaminated by water. Also, the degradation of mechanical properties may be observed after a long cycling process because of potential uneven Zn stripping/plating in the 3D network, which should be investigated in the future.

Conclusions

We employed ionic-liquid (EMIMTFSI) based gel polymer (PVDF-HFP) as the ionic conductive binder to make the flexible 3D Zn/AB/PVDF-HFP electrode which has good contact with the gel polymer electrolyte. The high effective surface area of the 3D Zn/AB/PVDF-HFP electrode can not only provide high electrochemical active surface area (~ 26 times higher than Zn metal plate) but also guarantee dendrite-free Zn plating at high geometric currents (up to $10 \text{ mA cm}^{-2}_{\text{geo}}$). With inert ionic liquid-based gel polymer electrolyte, the Zn/AB/PVDF-HFP electrode exhibited excellent stability ($> 800 \text{ h}$ cycling time) at high current (1, 2, 4, and $10 \text{ mA cm}^{-2}_{\text{geo}}$). This new Zn anode design provides a new way to overcome the poor interface with the gel polymer electrolytes and demonstrate stable rechargeable Zn metal batteries.

Acknowledgments

This work is supported by Toyota Motor Corporation (TMC).

ORCID

Yang Shao-Horn  <https://orcid.org/0000-0001-8714-2121>

References

- J. Liu et al., *Nat. Energy*, **4**, 180 (2019).
- W. Xu and Y. Wang, *Nano-Micro Lett.*, **11**, 90 (2019).
- S. J. Banik and R. Akolkar, *J. Electrochem. Soc.*, **160**, D519 (2013).
- Z. Liu, T. Cui, G. Pulletikurthi, A. Lahiri, T. Carstens, M. Olschewski, and F. Endres, *Angew. Chem. Int. Ed.*, **55**, 2889 (2016).
- F. Wang, O. Borodin, T. Gao, X. Fan, W. Sun, F. Han, A. Faraone, J. A. Dura, K. Xu, and C. Wang, *Nat. Mater.*, **17**, 543 (2018).
- J. F. Parker, I. R. Pala, C. N. Chervin, J. W. Long, and D. R. Rolison, *J. Electrochem. Soc.*, **163**, A351 (2016).
- J. F. Parker, C. N. Chervin, I. R. Pala, M. Machler, M. F. Burz, J. W. Long, and D. R. Rolison, *Science*, **356**, 415 (2017).
- J. Zheng et al., *Science*, **366**, 645 (2019).
- Y. G. Zhu et al., *Sustainable Energy Fuels*, **4**, 44076 (2020).
- G. Garcia, E. Ventosa, and W. Schuhmann, *ACS Appl. Mater. Interfaces*, **9**, 18691 (2017).
- X. Ren, S. Chen, H. Lee, D. Mei, M. H. Engelhard, S. D. Burton, W. Zhao, J. Zheng, Q. Li, and M. S. Ding, *Chem*, **4**, 1877 (2018).
- H. Jia, L. Zou, P. Gao, X. Cao, W. Zhao, Y. He, M. H. Engelhard, S. D. Burton, H. Wang, and X. Ren, *Adv. Energy Mater.*, **9**, 1900784 (2019).
- Z. Du, Y. Su, Y. Qu, L. Zhao, X. Jia, Y. Mo, F. Yu, J. Du, and Y. Chen, *Electrochim. Acta*, **299**, 19 (2019).
- F. Baskoro, H. Q. Wong, and H.-J. Yen, *ACS Appl. Energy Mater.*, **2**, 3937 (2019).
- D. Lei, Y.-B. He, H. Huang, Y. Yuan, G. Zhong, Q. Zhao, X. Hao, D. Zhang, C. Lai, and S. Zhang, *Nat. Commun.*, **10**, 1 (2019).
- C. Luo, T. Shen, H. Ji, D. Huang, J. Liu, B. Ke, Y. Wu, Y. Chen, and C. Yan, *Small*, **16**, 1906208 (2020).
- S. Ghorai, A. Sarkar, M. Raoufi, A. B. Panda, H. Schönherr, and S. Pal, *ACS Appl. Mater. Interfaces*, **6**, 4766 (2014).
- H. Li et al., *ACS Nano*, **12**, 3140 (2018).
- J. P. Tafur, J. Abad, E. Román, and A. J. Fernández Romero, *Electrochem. Commun.*, **60**, 190 (2015).
- H. Ohno, *Electrochemical aspects of ionic liquids*. (New York, NY)(Wiley) (2005).
- P. Yu, Y. Zeng, H. Zhang, M. Yu, Y. Tong, and X. Lu, *Small*, **15**, 1804760 (2019).
- J. Fu, D. U. Lee, F. M. Hassan, L. Yang, Z. Bai, M. G. Park, and Z. Chen, *Adv. Mater.*, **27**, 5617 (2015).
- Z. Wang, X. Meng, Z. Wu, and S. Mitra, *J. Energy Chem.*, **26**, 129 (2017).
- K. Wongrujipairoj, L. Poolnapol, A. Arpornwichanop, S. Suren, and S. Kheawhom, *Phys. Status Solidi (b)*, **254**, 1600442 (2017).
- S.-I. Hsiu, J.-F. Huang, I. W. Sun, C.-H. Yuan, and J. Shiea, *Electrochim. Acta*, **47**, 4367 (2002).
- W. Sun et al., *Science*, **371**, 46 (2021).
- M. Cui, J. Fei, F. Mo, H. Lei, and Y. Huang, *ACS Appl. Mater. Interfaces*, **13**, 54981 (2021).
- C.-H. Du, B.-K. Zhu, and Y.-Y. Xu, *J. Mater. Sci.*, **41**, 417 (2006).
- J. Liu, Z. Khanam, R. Muchakayala, and S. Song, *J. Mater. Sci., Mater. Electron.*, **31**, 6160 (2020).
- J. Liu, S. Ahmed, Z. Khanam, T. Wang, and S. Song, *Polymers*, **12**, 1755 (2020).
- G. G. Kumar and S. Sampath, *Solid State Ion.*, **160**, 289 (2003).
- X. Fan, J. Liu, Z. Song, X. Han, Y. Deng, C. Zhong, and W. Hu, *Nano Energy*, **56**, 454 (2019).
- B. Qiao et al., *ACS Cent. Sci.*, **6**, 1115 (2020).
- H. Gupta and R. K. Singh, "Ionic Liquid-based Gel Polymer Electrolytes For Application in Rechargeable Lithium Batteries." *Energy Storage Battery Systems - Fundamentals and Applications* (IntechOpen, London, UK) (2020), Energy Storage Battery Systems - Fundamentals and Applications .
- A. Noda, K. Hayamizu, and M. Watanabe, *J. Phys. Chem. B*, **105**, 4603 (2001).
- T.-Y. Wu, L. Hao, P.-R. Chen, and J.-W. Liao, *Int. J. Electrochem. Sci.*, **8**, 2606 (2013).
- C. Ferrara, V. Dall'Asta, V. Berbenni, E. Quartarone, and P. Mustarelli, *J. Phys. Chem. C*, **121**, 26607 (2017).
- J. P. Tafur and A. J. Fernández Romero, *J. Membr. Sci.*, **469**, 499 (2014).
- X. Zeng et al., *Adv. Mater.*, **33**, 2007416 (2021).
- C.-Y. Chen, K. Matsumoto, K. Kubota, R. Hagiwara, and Q. Xu, *Adv. Energy Mater.*, **9**, 1900196 (2019).
- N. Zhang, Y. Dong, Y. Wang, Y. Wang, J. Li, J. Xu, Y. Liu, L. Jiao, and F. Cheng, *ACS Appl. Mater. Interfaces*, **11**, 32978 (2019).
- Y. Cui et al., *Energy Storage Mater.*, **27**, 1 (2020).
- J. Huang, X. Chi, Y. Du, Q. Qiu, and Y. Liu, *ACS Appl. Mater. Interfaces*, **13**, 4008 (2021).
- V. Yufit, F. Tariq, D. S. Eastwood, M. Biton, B. Wu, P. D. Lee, and N. P. Brandon, *Joule*, **3**, 485 (2019).